

Accidental degeneracy beats: A distinct type of beat phenomenon in nonlinear optical spectroscopy

K. A. Merchant, David E. Thompson, and M. D. Fayer

Department of Chemistry, Stanford University, Stanford, California 94305

(Received 5 September 2001; published 17 January 2002)

A type of beat in nonlinear optical spectroscopy that is distinct from quantum beats (QB's) and polarization beats, is described. Like a quantum beat, this beat, which we refer to as an accidental degeneracy beat (ADB), can only be seen in multilevel systems. However, unlike quantum beats, which are the result of intramolecular interferences, ADB's are interferences between different subensembles of molecules in the sample. They require multilevel systems with spectral overlap. ADB's can appear as separate frequencies or as phase and amplitude contributions with the same frequency as that of quantum beats. A procedure for distinguishing between quantum beats and ADB's is outlined, and criteria under which ADB's are expected to be observed are delineated. Calculations of the spectrally resolved stimulated vibrational echo signal from an inhomogeneously broadened coupled anharmonic oscillator system are presented to illustrate the differences between the two types of beats. ADB's carry information about the anharmonicity of a system, while QB's carry information about intramolecular correspondence of transition frequencies in a multilevel system.

DOI: 10.1103/PhysRevA.65.023817

PACS number(s): 42.50.Fx, 42.50.Md, 42.50.Ct

I. INTRODUCTION

There are an increasing number of experiments that use coherence to probe the structure and dynamics of molecular systems [1–9]. The common feature in all these experiments is the generation of superpositions of states that evolve coherently. When more than two levels are involved, the possibility of interference between these coherent processes arises. The effects of such interferences have been seen in a wide variety of optical experiments, including fluorescence spectroscopy [10,11], photon-echo techniques [12–17], transient grating experiments [12,18,19], pump-probe spectroscopy [20–22], and Raman spectroscopy [23,24]. Regardless of the technique, multistate interferences inevitably lead to oscillations in the amplitude of the detected signal. Quantum beats (QB's) are one class of interferences that can produce these oscillations [10,14]. These beats are due to quantum-mechanical interference between the different system-evolution pathways that lead to the same final state. However, not all interference effects that have been observed in coherence experiments are due to quantum beats. Another class of interference effects, which we will refer to as accidental degeneracy beats (ADB's), has recently been observed in ultrafast infrared vibrational echo experiments [25–27]. These are a different type of beat, distinct from both QB's and polarization beats [28] that have been reported in other systems. ADB's are similar in appearance to QB's, but are the result of a very different microscopic mechanism and, as such, have different information content than QB's. Thus, it becomes necessary to have a clear understanding of how ADB's occur, when they are present, and what information they carry.

The similarities and differences between polarization beats, QB's and ADB's can be illustrated by comparing the nature of signals that can be generated in a vibrational echo experiment [29]. The stimulated vibrational echo [30] is the infrared analog of the three-pulse spin echo in nuclear magnetic resonance [31] and the three-pulse photon echo [4] in electronic excited state spectroscopy. The stimulated echo is

used to extract information contained in the dynamical line-width of a transition. In principle, this information is present in a linear absorption spectrum [32,33]. However, in transitions that are inhomogeneously broadened, it is difficult or impossible to extract meaningful dynamical information. Stimulated echo techniques remove inhomogeneous broadening and permit the observation of dynamical line shapes [33].

In this technique, three pulses with wave vectors \vec{k}_1 , \vec{k}_2 , and \vec{k}_3 and variable delays τ (between pulses 1 and 2) and T_w (between pulses 2 and 3) are crossed in a sample. In a massively inhomogeneously broadened sample, a new field is generated at a time $2\tau + T_w$ in the $\vec{k}_s = \vec{k}_2 + \vec{k}_3 - \vec{k}_1$ direction [34]. Consider an inhomogeneously broadened two-level system with center frequency ω_o . After the interaction with \vec{k}_1 , a macroscopic polarization is created in the sample as all oscillators in the system are brought into a coherent superposition of the ground and excited states. As each oscillator evolves in time at its natural transition frequency ω_i , which denotes its frequency relative to the line center ω_o , the macroscopic polarization undergoes a free induction decay (FID) at frequency ω_o as each oscillator dephases relative to the rest of the oscillators in the inhomogeneous system. After a time τ , the system interacts with the second pulse, driving the system from the coherence state into either the ground or excited population states (see Fig. 1, type-I diagrams). After another time T_w , the third pulse interacts with the system, taking it from either the ground or excited state back into a coherent superposition. Once again, each oscillator evolves at its natural transition frequency, but the sign of the coherence is opposite. The system now rephases at the frequency $-\omega_o$. As the entire ensemble of molecules rephase, a macroscopic polarization is recreated in the sample. This macroscopic polarization is responsible for the generation of the echo signal. At a time τ after the third pulse, the inhomogeneous dephasing that occurred for each oscillator during the period τ between the first pulse and second pulse is completely undone, and the intensity of the echo pulse is maxi-

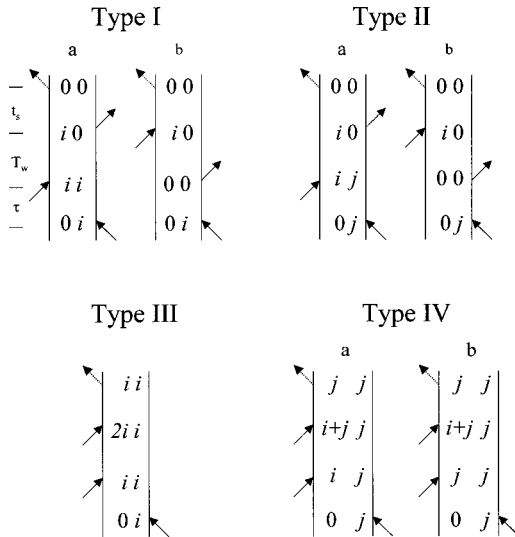


FIG. 1. Feynman diagrams that are involved in the calculation of the echo signal. The times after the first, second, and third interactions are τ , T_w , and t_s , respectively. For a two-level system, the type-I diagrams describe the echo response. For a three-level system that generates QB's, type-I and type-II diagrams must be considered together. For a three-level system that produces ADB's because of vibrational anharmonicity, type-I and type-III diagrams contribute to the total signal. For a coupled anharmonic oscillator [coupled vibrational local modes that give rise to two normal modes, S (symmetric) and A (antisymmetric), the anharmonic oscillator being one of them], types I–IV all participate in the generation of the overall echo response. These Feynman diagrams give the response from a single manifold. For example, for the S manifold, $i=S$, $j=A$. For the A manifold, $i=A$, $j=S$. The total echo signal for coupled anharmonic oscillators (S and A) contains 14 diagrams, 7 from the S manifold and 7 from the A manifold.

mum. At this point, the system undergoes another FID. These back-to-back FID's give rise to the temporally narrow echo wave packet. Over the course of the temporal evolution of the system, interactions between the oscillators and their environments give rise to processes that cause both excited-state relaxation and small stochastic phase variations in each oscillator's frequency. The excited-state relaxation reduces the amplitude of the echo wave packet by reducing the number of oscillators that generate the signal, and the accumulation of irreversible phase differences prevents perfect rephasing of the oscillators. As the delay times τ or T_w are increased, more of these decay events occurs, which gives rise to a decay in the echo signal as a function of these delays.

Consider a sample that has two possible inhomogeneously broadened transition frequencies; for example, the sample could be an impurity molecule in a molecular crystal that can occupy two different crystal sites with similar transition frequencies, or a molecule with two uncoupled transitions with similar frequencies, or a sample containing two different species but with similar transition frequencies. Now consider the results of performing an echo experiment on this sample. For the sake of clarity $T_w=0$, that is, the second and third pulses are time coincident. Upon coherent excitation of the sample with a pulse having sufficient bandwidth to drive both tran-

sitions simultaneously, an echo wave packet is generated by the sample that is the sum of the echo wave packets from each transition. If a fast photodetector capable of time resolving the envelope function of the wave packet is used, for a given delay τ , the detector will see an envelope function width that is related to the linewidths of the transitions and modulations at the difference frequency between the two transitions [28]. The signal is the result of the sum of the two individual contributions to the total polarization, and the modulations in the envelope of the echo wave packet are from the interference at the detector of the two distinct frequencies generated by the sample. This is what is commonly called a polarization beat [28], because it is a beat between the electric fields produced by the two polarizations generated in the sample. If a slow photodetector is used for detection (or equivalently, if the signal from the fast detector is integrated) and the signal is plotted as a function of the delay τ , then the echo curve will decay monotonically with no oscillations, regardless of the difference in transition frequency energy, the extent of inhomogeneous broadening, or overlap of the spectral lines. In a two-level system, the frequency at which an oscillator dephases is equal to the frequency at which it rephases. Therefore, the phase differences that accumulated between individual oscillators in the sample after the first pulse are undone during the time after the third pulse, and every oscillator has the same phase relationship when the echo wave packet is generated. The echo decay curve, therefore, shows no oscillations. If a fast photodetector is used to detect the echo signal at a single frequency by dispersing the signal with a monochromator, then the echo pulse envelope shows no oscillations; the integrated signal from each transition decays monotonically with increasing τ , consistent with a description of the oscillations seen in the time-resolved nonspectrally dispersed signal as an interference between two frequencies on the detector. The beat on the echo envelope (not spectrally resolved) is a polarization beat.

Now consider a different type of sample that is composed of a molecule with a ground state and two excited states that have similar energies and are both radiatively coupled to the ground state with transition frequencies ω_i and ω_j . The type-I and type-II Feynman diagrams in Fig. 1 describe the echo signal from such a system. If the transition frequencies and transition probabilities of this second type of sample lead to an absorption spectrum that is the same as the absorption spectrum from the first sample type, then (except for absolute amplitude) the temporally resolved echo envelope from the second sample type will be the same as from the first. However, if the integrated signal is plotted as a function of the delay τ , oscillations at the transition frequency difference, $\Delta\omega=|\omega_i-\omega_j|$ are observed in the echo decay curve as τ is increased. If one of the transitions is detected through a monochromator, then the temporally resolved envelope at a single τ position shows no modulations, but the integrated detector response as a function of τ shows oscillations at $\Delta\omega$ [3,35]. The same holds true if the other transition is detected through the monochromator. The interference between two different frequencies on the detector cannot apply in the spectrally resolved situation. Rather, the signal amplitude of

each frequency in the sample is being modulated as a function of the delay τ and at a frequency $\Delta\omega$. This is a quantum beat.

The explanation for the quantum-beat oscillations lies in the manner in which the coherent states are prepared and evolve. For the spectrally resolved signal, the detector sees signal from all oscillators that have their emission frequency (i.e., the coherence frequency after the third pulse) equal to the detection frequency of the monochromator ω_d . In general, the “state” of a time-evolving system is a superposition of all the quantum pathways that a particular system can follow. In the case of the coupled oscillator, there are multiple quantum pathways that lead to the same final coherence state with the coherence frequency equal to ω_d (see Fig. 1, type-I and -II diagrams). Assume that the monochromator is tuned to the transition with the transition frequency ω_i , so that $\omega_d = \omega_i$. In the quantum pathways represented by the type-I diagrams, the coherence frequency after the first interaction is ω_i and after the third interaction it is $-\omega_i$. In a two-level system, these are the only quantum pathways that need be considered. However, in the coupled oscillator case, the quantum pathways represented by the type-II diagrams must also be included in the final signal. These diagrams have a final coherence frequency of $-\omega_i$, but initially dephased at ω_j . Because the type-I and type-II quantum pathways have different initial coherence frequencies, there is a relative phase difference between them equal to $(\Delta\omega) \cdot \tau$. Since the type-I and type-II diagrams rephase at the same frequency, the phase difference $(\Delta\omega) \cdot \tau$ acquired during the first coherence period is not reversed after the third interaction. As τ is increased, the systematic phase difference between the type-I and type-II diagrams grows, and the final coherence states from the two sets of diagrams move in and out of the phase with each other. The τ -dependent phase difference gives rise to QB oscillations in the echo decay at a frequency $\Delta\omega$ as a function of τ , giving rise to oscillations in both the spectrally resolved and nondispersed echo decay curves.

To illustrate the nature of accidental degeneracy beats, consider a third type of sample composed of an inhomogeneously broadened weakly anharmonic oscillator [17]. In such a system, each energy level is strongly coupled by the radiation field only to adjacent energy levels. We define the transition frequencies between levels 0 and 1 as ω_i and between levels 1 and 2 as ω_{2i} , and the anharmonicity of the overtone as $\Delta_0 = |\omega_i - \omega_{2i}|$. There is no direct radiative coupling between the ground state and second excited state. The relevant quantum pathways for the generation of echo signal are given in Fig. 1, type-I and type-III Feynman diagrams. The echo signal is spectrally resolved through a monochromator tuned to the detection frequency ω_d . If the extent of inhomogeneous broadening is sufficient to cause overlap between the 0–1 and 1–2 lines, then it is possible for a subensemble of the molecules “A” to have $\omega_{iA} = \omega_d$ and a different subensemble of molecules “B” to have $\omega_{2iB} = \omega_d$. For the subensemble of molecules with $\omega_{2iB} = \omega_d$, the corresponding fundamental vibrational frequency is $\omega_{iB} = \omega_d + \Delta_0$. The B subensemble has its 0–1 transition frequency Δ_0 to the blue of ω_d , therefore, its 1–2 transition frequency

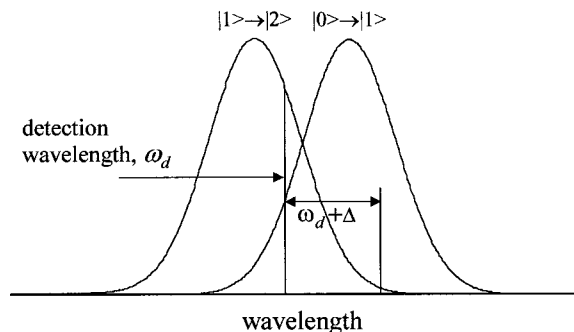


FIG. 2. A schematic illustration of the inhomogeneously broadened envelopes of a vibration’s 0–1 transition and the anharmonically shifted 1–2 transition as a function of the transition frequency. The vertical lines represent the 0–1 transition frequencies of the two distinct subensembles that contribute to the echo at the noted detection frequency ω_d . Anharmonic ADB’s arise because the type-I quantum pathway from subensemble A, which originates and emits on the red side (left side) of the 0–1 band at ω_d , interferes with the type-III quantum pathway of subensemble B that originates on the blue side of the 0–1 band at $\omega_d + \Delta$ (Δ is the vibrational anharmonicity) and emits from the blue side of the 1–2 band at ω_d .

is shifted to the red by the anharmonicity, Δ_0 , and is at ω_d . (See Fig. 2.) The type-I quantum pathway dephases and rephases at the same frequency. The type-I pathway of the subensemble A dephases at ω_d and rephases at $-\omega_d$. The type-III quantum pathway dephases and rephases at different frequencies. The type-III pathway of subensemble B dephases at $\omega_d + \Delta_0$ and rephases at $-\omega_d$. Since the type-I pathway of the subensemble A and type-III pathway of the subensemble B both rephase at the same frequency, they emit at the same frequency, ω_d . Relative to the type-I pathway of the subensemble A, the type-III pathway of the subensemble B has a phase difference equal to $\Delta_0 \cdot \tau$. Similar to quantum beats, this systematic phase difference advances as τ is increased and gives rise to amplitude modulations in the integrated intensity of individual frequencies as a function of the delay time [26]. However, unlike quantum beats, which involve intramolecular interferences that occur within every oscillator in the sample, ADB’s occur due to interferences between distinct subensembles that follow different quantum pathways and that have overlapping emission lines. A previous explanation of this type of oscillation in echo decays has attributed the modulations to interference between two different frequencies on the detector [36]. Clearly, this explanation cannot apply in the spectrally resolved situation. Rather, the signal amplitude of each emission frequency for which spectral overlap occurs, is being modulated as a function of the delay τ and at a frequency Δ_0 [26]. In this example, inhomogeneous broadening is the process that gives rise to the emission frequency overlap. Other possible mechanisms can lead to ADB’s. These will be discussed below.

Accidental degeneracy beats are a type of beat that are distinct from both polarization beats and quantum beats. Similar to polarization beats, they are the result of an interference between different subensembles within the sample. However, while polarization beats do not produce modulations at the difference in transition frequencies in echo decay

curves, ADB's do produce such modulations. Like quantum beats, ADB's present even when the echo signal is dispersed in a monochromator and an arbitrarily narrow bandwidth is detected.

Despite their similarities, ADB's are distinct from quantum beats, and they carry different information content than quantum beats. A *quantum beat* is defined to be an *intramolecular interference effect* where an oscillator can evolve along different quantum pathways with different coherence frequencies but *the termini of the pathways are the same final state with the same final coherence frequency*. This interference effect occurs in each oscillator in the ensemble. A quantum beat is an intramolecular process. An *accidental degeneracy beat* is defined to be an interference effect *between distinct subensembles* of the system, which evolve along different quantum pathways with different coherence frequencies and *the termini of the pathways are different final states but have the same final coherence frequency*. Owing to the spectral line overlap caused by inhomogeneous broadening or other mechanisms, the subensembles have the same final coherence frequency (same emission frequency). The ADB interference effect does not occur in every oscillator in the system. Rather, only those subensembles of molecules that have an emission frequency that overlaps with other spectroscopic lines will produce an ADB. For both ADB's and QB's, it is incorrect to think of the observed beats as interference between different frequencies on the detector.

In this paper, a model inhomogeneously broadened coupled anharmonic oscillator system is used to examine the difference between QB's and ADB's as manifested in a spectrally resolved stimulated vibrational echo experiment. Calculations are presented that illustrate the influence of ADB's on decays when either τ or T_w is scanned. While the calculations pertain explicitly to vibrational echo experiments, the differences between QB's and ADB's and the conclusions that can be drawn about these two types of beats are quite general and apply to a wide variety of spectroscopies.

II. THEORY

In vibrational systems, pulses with durations that are short enough to extract dynamical information from a system frequently have bandwidths that exceed the anharmonicity of the vibrational transition and the splitting between coupled modes. This can lead to complex oscillatory patterns in echo decay curves, since coherences between many different levels are possible, with many possible quantum pathways that lead to the same final emission frequency. As the delay times τ or T_w are scanned, systematic phase differences between a multitude of quantum pathways arise and advance leading to the complicated oscillatory patterns that have been observed in vibrational echo experiments [3,15].

The coupled anharmonic oscillator presented here has six levels that can be accessed at third order. An energy level diagram for such a system is shown in Fig. 3. There is a ground state, two vibrational fundamentals (which will be referred to as a symmetric S and antisymmetric A stretch [37]), an overtone for each fundamental, and a combination

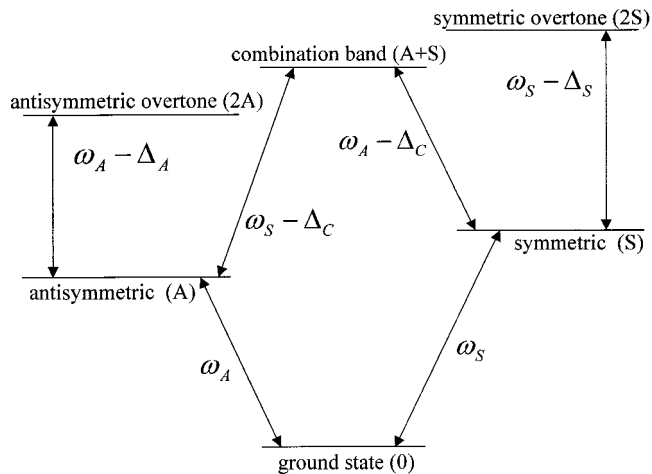


FIG. 3. Energy-level diagram for a coupled anharmonic oscillator system. The lowest six energy levels are shown. The arrows indicate allowed transitions. The transition frequencies are indicated next to each arrow. ω_S and ω_A are the symmetric and antisymmetric transition frequencies. Δ_C , Δ_S , and Δ_A are the combination band shift, symmetric overtone anharmonicity, and antisymmetric overtone anharmonicity, respectively. Designations of the energy levels are given in parentheses next to the level name.

band. The double-headed arrows indicate allowed transitions. In a linear absorption spectrum, the overtone and combination band absorptions for such a system appear as small features at approximately twice the frequency of the fundamental transitions. These are due to weakly allowed direct transitions between the ground state and the overtone and combination band levels. In nonlinear experiments, the excitation pulses do not usually have sufficient bandwidth to drive both the fundamental and overtone transitions directly. Instead, the overtone and combination band levels are accessed from the fundamental excited states. These transitions are all strongly allowed and appear at approximately the same energy in the spectrum.

Fourteen Feynman diagrams must be considered in computing the echo signal for this system. Each diagram represents one contribution to the final state of the molecule after the interactions with the field. The state of each molecule after the third interaction with the field is the superposition of all the final states of the diagrams. Seven Feynman diagrams, shown in Fig. 1, describe the evolution of the system as it emits from the symmetric S vibrational state, and seven diagrams describe the pathways that lead to an emission from the antisymmetric A vibrational state. These sets of seven diagrams can be further categorized into four types. Type I are diagrams that involve only the ground and first excited state of one manifold. Type II are diagrams that involve the first excited states of the S and A manifolds. Type-III diagrams involve the three lowest levels ($v=0, 1$, and 2 , with v the vibrational quantum number) of one manifold; and type-IV diagrams are diagrams that involve both manifolds and the combination band. There are two diagrams of each type with the exception of type III. It is important to note that in the absence of both coupling and anharmonicity, type-II and type-IV diagrams will destructively interfere at

all times, and in the absence of anharmonicity, type I and type III will destructively interfere at all times, resulting in no nonlinear signal [38,39].

There are three time periods during which the system evolves. These are the periods τ after the first interaction (first pulse), the period T_w after the second interaction (second pulse), and the detection period t_s after the third interaction (third pulse). In a traditional stimulated echo experiment, the integrated signal is recorded while one of the two time periods, τ or T_w , is held fixed and the other is scanned [40]. This gives control over two of the three coherence times. Information about the detection period t_s is obtained by measuring the spectrum of the generated signal. The frequency spectrum of the signal pulse gives the amplitude information about each frequency, but the relative phase of each frequency is not resolved by the square-law detector. To obtain complete information about the evolution of the system during the third time period, it is necessary to mix the generated field with a local oscillator as a function of time (heterodyne detection [4,41]) or to mix the signal with a local oscillator in a monochromator (spectral interferometry [42,43]). However, for the purposes of understanding the ADB phenomena, the absolute phase of the generated signal is not needed, and it is sufficient to spectrally resolve the generated signal. Because there are two distinct time periods that can be scanned, beats that are observed as τ is scanned (τ -dependent beats) and beats that are observed as T_w is scanned (T_w -dependent beats) are treated separately. This is a useful distinction because the number and type of beats that are produced in each situation is different, and, depending on the process of interest, has implications for the design of experiments.

The behavior of the three-pulse vibrational echo signal for a τ -dependent scan will be analyzed first. To simplify the explanation, consider the beats that are on the S manifold only (the analysis of the A manifold is completely equivalent). Because the vibrational echo signal is spectrally resolved, only a narrow band of frequencies is measured at any given time. Therefore, the *emission frequencies* ω_e , which are the same as the third coherence frequency of each diagram, are all required to be identical (within the monochromator detection bandwidth). (Note that this does not necessarily place a restriction on the final state.) The emission frequency is equal to the detection frequency of the monochromator, $\omega_e = \omega_d$. The four types of diagrams give rise to four distinct coherence states during the τ coherence period that lead to the emission frequency ω_e : ρ_{0S}^I , ρ_{0A}^{II} , ρ_{0S}^{III} , and ρ_{0A}^{IV} , where the subscript indicates the states involved in the coherence (see Fig. 3), and the superscript refers to the quantum pathway (see Fig. 1). Each density matrix element has associated with it a coherence frequency, which we denote in the same way. They are, respectively, ω_{0S}^I , ω_{0A}^{II} , ω_{0S}^{III} , and ω_{0A}^{IV} . The emission frequency (i.e., the rephasing frequency) of all of these pathways is the same. Any beats that are observed are the result of differences in the dephasing frequencies. Taking all possible combinations of the absolute value of differences between these frequencies gives $4!/(2!2!) = 6$ combinations of frequencies

$$\omega_A = |\omega_{0S}^I - \omega_{0A}^{II}|, \quad (1a)$$

$$\omega_B = |\omega_{0S}^I - \omega_{0S}^{III}|, \quad (1b)$$

$$\omega_C = |\omega_{0A}^{II} - \omega_{0S}^{III}|, \quad (1c)$$

$$\omega_D = |\omega_{0S}^I - \omega_{0A}^{IV}|, \quad (1d)$$

$$\omega_E = |\omega_{0A}^{II} - \omega_{0A}^{IV}|, \quad (1e)$$

$$\omega_F = |\omega_{0S}^{III} - \omega_{0A}^{IV}|. \quad (1f)$$

The next step is to determine which frequencies arise from quantum beats and which arise from accidental degeneracy beats. The test is straightforward. Examine each pair of coherence frequencies in Eqs. (1). If the diagrams that each pair belong to have the same final state, then the resulting oscillation at the frequency difference is a quantum beat. Of these six equations, only Eq. (1a) meets this requirement. The remaining five equations can give rise to accidental degeneracy beats. For these equations, the final states of the two contributing diagrams are different, but if there is overlap between the different transitions, then these oscillators can dephase at different coherence frequencies and rephase at the same one, producing a τ -dependent oscillation in the signal even though the signal is spectrally resolved. Similar to a quantum beat, the accidental degeneracy beats are produced in the sample and are not the result of interference on the detector. In general, not all five ADB frequencies will be observed in an echo experiment. In order to observe an ADB, there must be spectral overlap between the two different transitions that are responsible for the emission. Without spectral overlap, it is not possible to have subensembles that dephase at different frequencies and rephase at the same frequency. In contrast, quantum beats do not depend on spectral line overlap, because QB's are an intramolecular process. In a quantum beat, each individual oscillator produces a modulation in emission frequency as a function of τ . This fundamental distinction between the two mechanisms of the beats has important implications for the information content contained in their interferences.

Now consider the case for a T_w scan in which the delay between the first and second pulse is held fixed and the delay between the second and third pulses is varied. The procedure is the same as that used to analyze the τ -dependent beats. Listing all density matrix elements and their associated frequencies that evolve during the time period T_w and that lead to the emission frequency ω_e gives ρ_{SS}^I , ρ_{00}^I , ρ_{00}^{II} , ρ_{SA}^{II} , ρ_{SS}^{III} , ρ_{AA}^{IV} , and ρ_{SA}^{IV} with associated frequencies ω_{SS}^I , ω_{00}^I , ω_{SA}^{II} , ω_{SS}^{III} , ω_{AA}^{IV} , and ω_{SA}^{IV} . Of the seven density matrix elements listed here, only ω_{SA}^{II} and ω_{SA}^{IV} have nonzero frequencies associated with them. The remaining five frequencies are associated with population states that have zero frequency and undergo no phase evolution. (While these states do not have an associated frequency, they do have an initial phase, which can play an important role in the behavior of the observed oscillations. This is discussed in detail below.) Taking com-

binations of the absolute value differences between ω_{SA}^{II} , ω_{SA}^{IV} , and a zero frequency term gives $3!/(1!2!)=3$ beat frequencies

$$\omega_G = |\omega_{SA}^{\text{II}} - 0| = |\omega_{SA}^{\text{II}}|, \quad (2a)$$

$$\omega_H = |\omega_{SA}^{\text{II}} - \omega_{SA}^{\text{IV}}|, \quad (2b)$$

$$\omega_I = |\omega_{SA}^{\text{IV}} - 0| = |\omega_{SA}^{\text{IV}}|. \quad (2c)$$

Equations (2a) and (2c) are quantum beats at the frequencies expected in the type-II and type-IV quantum pathways of Fig. 1. [While the frequencies in Eqs. (2a) and (2c) are the true quantum-beat frequencies, the amplitude and phase of the oscillations in Eqs. (2a) and (2c) can be influenced by ADB phase and amplitude contributions to these oscillations, and it is, therefore, not correct to treat them as pure quantum beats. This is discussed further below.] The beats in Eqs. (2a) and (2c) are referred to as pseudo quantum beats. Equation (2b) is an ADB at the difference frequency between the two pseudo quantum-beat frequencies. Population state density matrix elements have zero frequency. Because they do not evolve in phase as T_w is changed, they do not give rise to systematic phase differences among coherence states at the emission frequency. Thus, there are fewer beat frequencies in the T_w -dependent scan than in the τ -dependent scan.

The above discussion is completely general, and makes no assumptions about the functional form of the energies for the coupled levels or the nature of inhomogeneous broadening. The only requirement has been the nonzero coupling and anharmonicity. To calculate the expected beat frequencies in a system, it is necessary to invoke a model of coupling and inhomogeneous broadening to determine the value of the coherence frequencies that lead to a particular emission frequency. We choose a bilinearly coupled harmonic oscillator system, and graft on anharmonicity phenomenologically. This model has been used successfully previously to describe two dimensional ultrafast vibrational echo experiments [3,44]. Starting with degenerate harmonic oscillators, the system is taken to have the following Hamiltonian:

$$\underline{H} = \underline{H}_\alpha + \underline{H}_\beta + \underline{H}_{\alpha\beta} + \underline{H}_{\alpha S} + \underline{H}_{\beta S}, \quad (3)$$

where \underline{H}_α and \underline{H}_β are the harmonic oscillator Hamiltonians for the two local modes that will combine to produce the S and A states. $\underline{H}_{\alpha\beta}$ represents the Hamiltonian that couples the two local modes to each other, and $\underline{H}_{\alpha S}$ and $\underline{H}_{\beta S}$ are Hamiltonians representing the coupling of the local modes to the solvent. The coupling between the local modes is modeled with bilinear coupling

$$\underline{H}_{\alpha\beta} = \gamma \underline{x}_\alpha \underline{x}_\beta, \quad (4)$$

where \underline{x}_i is the position operator and γ is the coupling strength between the modes. The coupling of the local modes to the solvent is not treated explicitly, but taken to give identical Gaussian distributions of local mode energies centered at the frequency ω_o and with the width σ . Ignoring terms that couple states that differ by two or more quanta of energy [45], and diagonalizing a 16×16 matrix to compute the lowest six eigenstates that enter into this discussion, leads to the following expressions for the energies:

$$E_0 = \frac{1}{2} \hbar (\omega_\alpha + \omega_\beta), \quad (5a)$$

$$E_A = \hbar (\omega_\alpha + \omega_\beta) - \frac{\hbar}{2} \delta, \quad (5b)$$

$$E_S = \hbar (\omega_\alpha + \omega_\beta) + \frac{\hbar}{2} \delta, \quad (5c)$$

$$E_{2A} = \frac{3}{2} \hbar (\omega_\alpha + \omega_\beta) - \hbar \delta, \quad (5d)$$

$$E_{A+S} = \frac{3}{2} \hbar (\omega_\alpha + \omega_\beta), \quad (5e)$$

$$E_{2S} = \frac{3}{2} \hbar (\omega_\alpha + \omega_\beta) + \hbar \delta, \quad (5f)$$

with

$$\delta = \sqrt{\gamma^2 / (\mu^2 \omega_\alpha \omega_\beta) + (\omega_\alpha - \omega_\beta)^2}, \quad (6)$$

where ω_α and ω_β are the local mode frequencies and μ is the reduced mass of a local mode. These eigenenergies correspond to the ground, antisymmetric, symmetric, antisymmetric overtone, combination band, and symmetric overtone energies, respectively (Fig. 3). Because the basis functions used in this diagonalization are harmonic, the resultant eigenstates and eigenenergies are also harmonic. Real molecular vibrational oscillators are anharmonic, and it is necessary to include anharmonicity to produce a nonlinear signal. We do this below phenomenologically by introducing anharmonicity and combination band shift values to Eqs. (5c) and (5f).

Equations (5c)–(5f) allow the computation of all transition frequencies for a molecule with a given set of local mode parameters. This allows us to correlate the transition frequency in one spectroscopic line to the transition frequency in another line [46]. However, a model for the inhomogeneous distribution of transition frequencies within a spectroscopic line is still needed. There are three variable input parameters for the eigenenergies in Eqs. (5) that can be used to broaden the spectroscopic lines: γ , ω_α , and ω_β . Fluctuations in γ will produce S and A inhomogeneous lines that have equal width, and transition frequencies that are anticorrelated, that is, as the S transition frequency for a molecule increases, the A frequency decreases [3,44]. Another possible mechanism for the inhomogeneous broadening is variations in local mode frequencies ω_α and ω_β . If solvent perturbations to the local mode oscillator produce local effects, ω_α and ω_β will vary independently in an uncorrelated manner [3]. Alternatively, if solvent perturbations cause global changes in the molecule, the frequency of the local modes ω_α and ω_β will vary in a correlated fashion [3,44]. For the sake of simplicity, we take the local mode frequencies ω_α and ω_β to be completely correlated, namely $\omega_\alpha = \omega_\beta = \omega$, and assume that the inhomogeneous broadening is due to variations in the local mode frequency ω . (This model is consistent with previously reported experimental results [3,44].) Then, the final expressions for the eigenenergies as a function of local mode parameters are

TABLE I. Beat frequency expressions and values for an inhomogeneously broadened bilinearly coupled anharmonic oscillator with perfectly correlated local mode energies. The beats are from Eqs. (1) and (2). δ , Δ_S , and Δ_C are defined in Eqs. (8), (7f), and (7e), respectively.

Beat	Type	Range	Expression	Value (cm ⁻¹)
ω_A	QB	0–1	2δ	$\sim 160^a$
ω_B	ADB	0–1/1–2 overlap	Δ_S	30
ω_C	ADB	0–1/1–2 overlap	$2\delta + \Delta_S$	$\sim 190^a$
ω_D	ADB	0–1/C band overlap	$2\delta - \Delta_C$	$\sim 90^a$
ω_E	ADB	0–1/C band overlap	Δ_C	70
ω_F	ADB	1–2 C band overlap	$2\delta - \Delta_C + \Delta_S$	$\sim 120^a$
ω_G	pseudo-QB	0–1	2δ	$\sim 160^d$
ω_H	ADB	0–1/C band overlap	$\omega_C - \omega_1$	$\sim 6^a$
ω_I	pseudo-QB	0–1	$2\delta^b$	$\sim 166^a$

^aThe exact value of the beat depends on the detection frequency.

^bThe δ in this expression has a different value of ω compared to the δ in the expressions for ω_A and ω_G .

$$E_0 = \hbar\omega, \quad (7a)$$

$$E_A = 2\hbar\omega - \frac{\hbar}{2}\delta, \quad (7b)$$

$$E_S = 2\hbar\omega + \frac{\hbar}{2}\delta, \quad (7c)$$

$$E_{2A} = 3\hbar\omega - \hbar\delta - \hbar\Delta_A, \quad (7d)$$

$$E_{A+S} = 3\hbar\omega - \hbar\Delta_C, \quad (7e)$$

$$E_{2S} = 3\hbar\omega + \hbar\delta - \hbar\Delta_S, \quad (7f)$$

with

$$\delta = \gamma/\mu\omega, \quad (8)$$

where Δ_A , Δ_C , and Δ_S are the antisymmetric overtone anharmonicity, the combination band shift, and the symmetric overtone anharmonicity, respectively. This is all that is needed to calculate actual beat frequencies for the model system. The emission frequencies for each diagram are required to be equal to each other. Next, Eqs. (7) and (8) are used to calculate the frequencies of the rest of the density matrix elements. All possible beat frequencies in the τ -dependent and T_w -dependent delay scans can then be calculated using Eqs. (1) and (2). The expressions for the beat frequencies expected in a system with correlated local mode frequencies are listed in Table I and are derived in Appendix A.

III. CALCULATIONS

To better see the differences between quantum beats and accidental degeneracy beats, and the magnitude of their contributions, the vibrational echo signal was calculated for echo scans in which τ and T_w are varied. The calculation employs δ -function excitation pulses and exponential dephasing and relaxation kinetics. The nature of the results does not depend on the duration of the excitation pulses or the form of the

dephasing. The triple integral over the excitation fields was done analytically for each diagram. The responses of each diagram were added, and the integral over the distribution of local mode energies was evaluated numerically. The resulting vibrational echo wave packet was Fourier transformed and the power spectrum computed to calculate the spectrally resolved signal.

One complication that occurs in calculations with δ -function pulses is that signals that would otherwise have smooth rising edges begin abruptly. If one performs a Fourier transform on a signal with such a discontinuity, then the sharp edge introduces spurious frequencies into the spectrum that are an artifact of the Fourier transform. In the context of stimulated echo calculations, there are two places where an abrupt rising edge causes spectral contamination of the calculated signal. One place is in the calculation of the vibrational echo wave packet at fixed values of τ and T_w . The other is in the integrated echo signal decay. In a δ -function pulse calculation, the rising edge of each Fourier component in the echo wave packet begins abruptly. In an exact calculation using realistic pulse durations for the excitation fields, this rising edge is related to the pulse duration. With δ -function pulses, at short times when the echo signal is not well separated from the free induction decay, this edge influences the shape of the echo wave packet. The contribution from a single diagram is a time-ordered triple integral that has the form [33]

$$P^{(3)}(t_s) \propto \int_{-\infty}^{t_3} dt_3 G_3(t_s - t_3) E_3(t_s - \tau - T_w) \int_{-\infty}^{t_3} dt_2 G_2 \times (t_3 - t_2) E_2(t_2 - \tau) \int_{-\infty}^{t_2} dt_1 G_1(t_2 - t_1) E_1(t_1) \quad (9a)$$

with

$$E_i(t) = \delta(t) \quad (9b)$$

and

$$G_i(t) = \exp[-i\omega_i t - \Gamma_i t], \quad (9c)$$

where ω_i is the transition frequency of the oscillator, G_i is the material Green's function propagator for the system, and Γ_i is the damping rate constant for a particular Green's function. Integrating over the excitation fields yields

$$P^{(3)}(t_s) \propto \theta(t_s - \tau - T_w) G_3(t_s - \tau - T_w) G_2(T_w) G_1(\tau) \quad (10a)$$

or writing G_3 explicitly

$$P^{(3)}(t_s) \propto \theta(t_s - \tau - T_w) \exp[-i\omega_3(t_s - \tau - T_w) - \Gamma_3(t_s - \tau - T_w)] G_2(T_w) G_1(\tau), \quad (10b)$$

where $\theta(t)$ is the Heaviside step function and reflects the causality of the system. The heaviside step function makes the signal turn on abruptly, which introduces spurious Fourier components that obscure the important features of the data. This artifact is only present at values of τ and T_w that are short compared to the FID time. This artifact can be prevented at all times by modifying G_3 in Eq. (10) slightly to go smoothly from zero to its maximum value at $t_s = \tau + T_w$ by replacing the time multiplying the damping rate by the absolute value of time and eliminating θ , allowing t_s to take on any value. With these modifications

$$P^{(3)}(t_s) \propto \exp[-i\omega_3(t_s - \tau - T_w) - \Gamma_3|t_s - \tau - T_w|] G_2(T_w) G_1(\tau). \quad (11)$$

At short times, this slightly modifies the decay of the echo signal. However, the feature of prime interest here are the beat frequencies that are present in the decay, not the shape of the decay at very short times. Because the extent of the error is limited only to short times, Eq. (11) is used in the calculations of the echo decay.

The two-dimensional (2D) vibrational echo spectrum was calculated as a function of delay line position. With δ -function pulses, the signal is zero for negative values of τ and T_w , and begins abruptly at zero. We wish to measure the beat frequencies present in the echo decay curve at a variety of frequencies by Fourier transforming slices along the time axis in the echo decay curves. The edge at zero time was removed by reflecting the signal at positive time back to negative time. Symmetrizing the data in this way removes the sharp rising edge in the decay curves, and gives accurate line shapes for the beat frequencies in the Fourier spectrum. This technique has an advantage over techniques using a windowing function [41,47] because the transformed data is not influenced by a convolution of the spectrum with the window function.

IV. RESULTS AND DISCUSSION

Figure 4 is an illustration of the three spectroscopic lines that compose one manifold and that overlap due to the inhomogeneous broadening. Underneath each spectrum is the type and range of each kind of beat seen in a τ -dependent scan [Fig. 4(a)] and T_w -dependent scan [Fig. 4(b)]. The ω_A

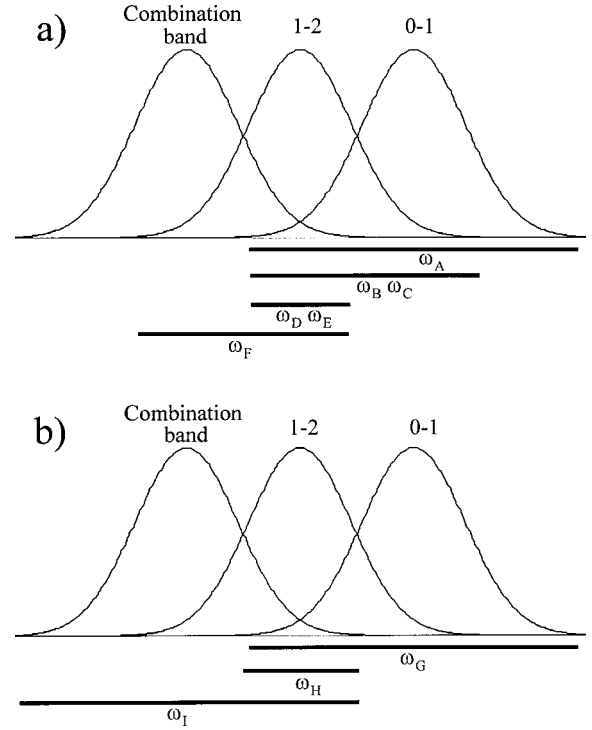


FIG. 4. The type of beats observed and the range of detection wavelengths for which they will be observed for the symmetric manifold. The three peaks are the 0–1 transition, the 1–2 transition, and the combination band. The beat frequencies listed here correspond to the ω_A through ω_I in Eqs. (1) and (2). (a) τ -dependent scan. Only ω_A is a true quantum beat. The remaining beats are accidental degeneracy beats. (b) T_w -dependent scan. ω_G and ω_I are pseudo-quantum-beats. ω_H is an accidental degeneracy beat. In both the τ -dependent and T_w -dependent cases, quantum beats will always be present in the data. Accidental degeneracy beats are only seen where there is spectral overlap. If there is no spectral overlap, then ADB's are not observed.

range in Fig. 4(a) is a quantum beat that extends over the entire 0–1 line, and corresponds to the quantum beat in Eq. (1a). The range spanned by ω_B and ω_C are ADB's seen only where the 0–1 and 1–2 line overlap. They correspond to Eqs. (1b) and (1c). ω_D and ω_E are ADB's that occur only where the 0–1 and combination band overlap. These beats will typically have the smallest amplitude and will be the hardest to see because the amplitude of the inhomogeneous lines where the 0–1 and combination bands overlap is low. They correspond to Eqs. (1d) and (1e). The range spanned by ω_F is the region of overlap between the 1–2 and combination band and corresponds to the ADB in Eq. (1f). In the places where several beat frequencies are present, the decay takes on a complex oscillatory pattern that is the result of these multiple beat frequencies. For example, all six beat frequencies are expected in the region where the 0–1, 1–2, and combination bands overlap.

Now consider the case for the T_w -dependent scan, illustrated in Fig. 4(b). Overall, there are only three frequencies expected. Three beat frequencies will occur simultaneously only in the region where the 0–1 line overlaps with combination band. The ω_G range extends over the 0–1 line and

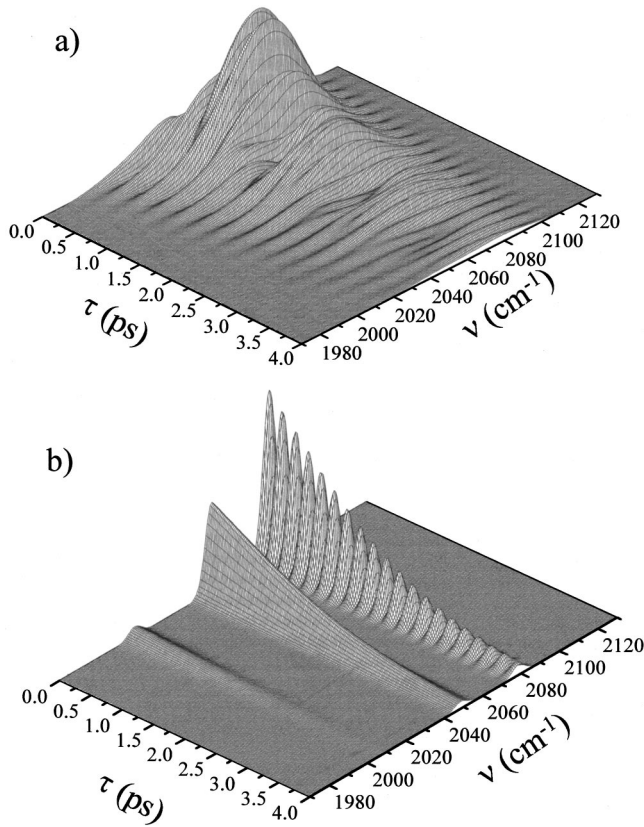


FIG. 5. Calculated spectrally resolved 2D vibrational echo signal for a τ -dependent scan ($T_w=0$). (a) Strongly overlapping 0–1, 1–2, and combination bands. The signal displays a complex oscillatory pattern composed of multiple frequencies over the entire line. (b) Well separated 0–1, 1–2, and combination band. Quantum beat oscillations are observed on the 0–1 line; there are no accidental degeneracy beats.

corresponds to the pseudo-quantum-beat in Eq. (2a) the ω_H range corresponds to the ADB in Eq. (2b) and the ω_I range corresponds to the pseudo-quantum-beat in Eq. (2c). While the beats in the ω_G range and ω_I range are not necessarily pure QB's, they are a single frequency.

Figures 5 and 6 present the results of calculations of the vibrational echo response for the signal generated in the S emission manifold of the coupled oscillator. In these calculations, the anharmonic shift is 30 cm^{-1} , the combination band shift is 70 cm^{-1} , and the splitting between the symmetric and antisymmetric lines is 160.4 cm^{-1} . Calculations were run for Gaussian local mode energy distributions with full width at half maxima of 70 cm^{-1} [Figs. 5(a) and 6(a)] and 15 cm^{-1} [Figs. 5(b) and 6(b)]. Figures 5(a) and 5(b) present the results of a τ -dependent scan for the S line in the case of large and small inhomogeneous broadening, respectively. The contributions from the 0–1, 1–2, and combination band are not well resolved in the case of large inhomogeneous broadening, and the signal decay exhibits a complicated oscillatory pattern. In the case of nonoverlapping peaks, the contribution from each peak is well resolved and oscillations are only seen on the 0–1 transition. In the absence of spectral overlap, there are no ADB's, and only the single QB occurs. Figures 6(a) and 6(b) present the results of a T_w -dependent

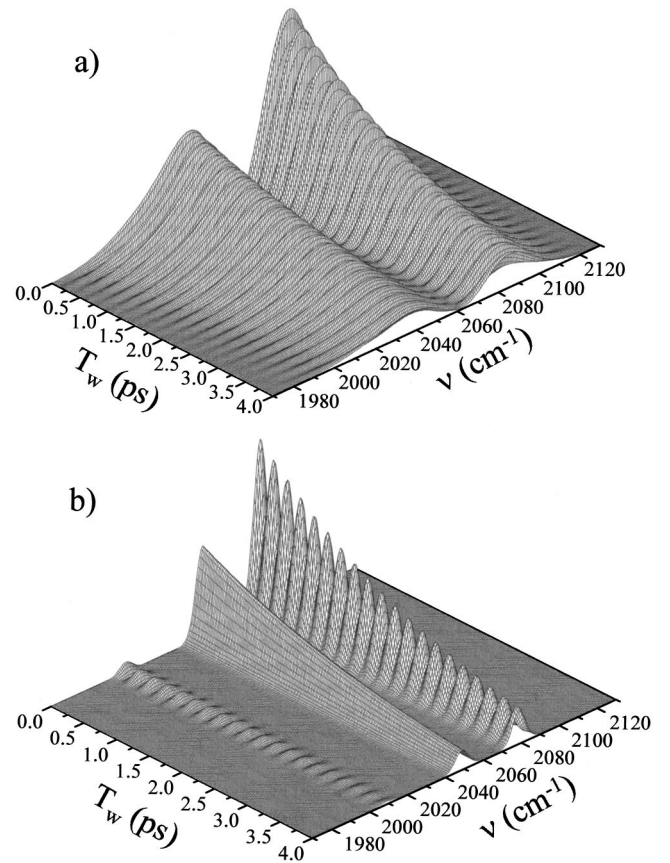


FIG. 6. Calculated spectrally resolved 2D vibrational echo signal for a T_w -dependent scan ($\tau=0$). (a) Strongly overlapping 0–1, 1–2, and combination bands. The signal displays a single oscillatory pattern over the entire line. (b) Well separated 0–1, 1–2, and combination band. Quantum beat oscillations are observed on both the 0–1 and combination band line.

scan for the S line with large and small inhomogeneous broadening. As is the case for a τ scan, when the inhomogeneous broadening is large [Fig. 6(a)], the three bands that contribute to the signal are not well resolved, but the nature of the decay is very different from the τ -dependent scan. Only one frequency is seen in the decay. In the case where the peaks are well resolved and do not overlap [Fig. 6(b)], oscillations are seen on both the 0–1 and combination bands.

Time slices through the curves in Figs. 5(a) and 6(a) at selected frequencies were extracted and Fourier transformed in the manner discussed above. These results are presented in Figs. 7 and 8, respectively. In Figs. 7(a)–7(e) the Fourier transforms of the time slices from Fig. 5(a) at 2120, 2100, 2050, 2040, and 2010 cm^{-1} show that there are numerous frequencies present, and that particular beat frequencies are only present at certain detection wavelengths. The quantum beat only appears on the 0–1 line. ADB's between diagrams that involve the 0–1 and 1–2 lines only appear at those frequencies where both the 0–1 and 1–2 lines overlap. A similar restriction is seen for all the ADB's. The amplitude of an ADB is related to the extent of overlap between two lines; if the lines do not overlap, then the amplitude of that ADB is zero. As can be seen in the calculations in Fig. 7, the

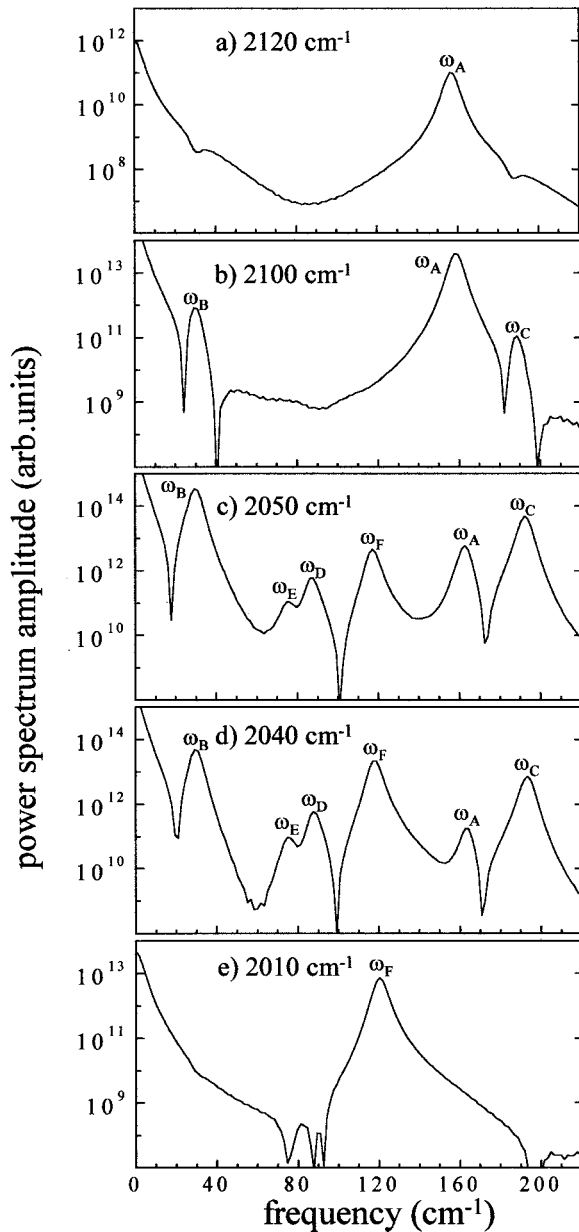


FIG. 7. Fourier transform of time slices at various detection frequencies from Fig. 5(a) (τ scan). The beat frequencies listed here correspond to the ω_A through ω_F in Eq. (1). Detection frequencies are (a) 2120 cm^{-1} . Only one beat frequency is seen. (b) 2100 cm^{-1} . This region has the 0–1 and 1–2 lines strongly overlapping. Three frequencies are seen. (c) 2050 cm^{-1} . All three spectroscopic lines are strongly overlapping. As predicted, six beat frequencies are seen. (d) 2040 cm^{-1} . Six frequencies are still seen, but the relative amplitude of each frequency is different than in (c). This is due to the different amplitudes of the inhomogeneous lines at this frequency. (e) 2010 cm^{-1} . Only the combination band ADB is seen.

quantum-beat frequency ω_A is not constant throughout the inhomogeneous line. The way in which the QB frequency changes with detection wavelength can be used to study the mechanism of inhomogeneous broadening [3]. Variations in the QB frequency with position in the inhomogeneous line have been observed experimentally [3].

There is a great deal of information contained in the os-

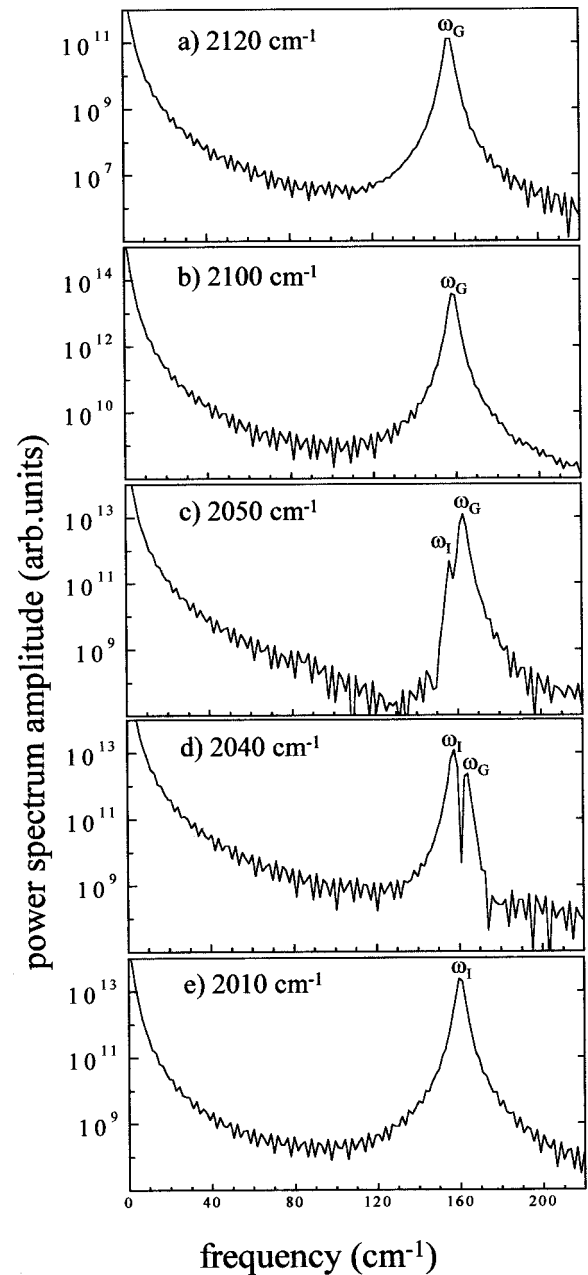


FIG. 8. Fourier transform of time slices at various detection frequencies from Fig. 6(a) (T_w scan). The beat frequencies listed here correspond to the ω_G through ω_I in Eq. (2). Frequency slices are the same as in Fig. 7. Detection frequencies are (a) 2120, (b) 2100, (c) 2050, (d) 2040, and (e) 2010 cm^{-1} . (a), (b), and (e) show only one beat frequency. In (c) and (d) where both the 0–1 and combination band overlap, pseudo-quantum-beats from the 0–1 line and the combination band can be seen. In addition, an ADB at $\sim 6 \text{ cm}^{-1}$ [ω_H in Eq. (2b)] is also present, but it is not discernible in this presentation of the data.

cillations seen in the data. In principle, there are four aspects of a beat that can provide information on molecular phenomena. These aspects are the frequency of the beat [10], the amplitude of the beat [48], that is, the depth of modulation, the initial phase of the beat [49], and the damping rate of the beat [3,46]. Quantum beats and accidental degeneracy beats

encode different types of information in these aspects of a beat. In a QB, the beat frequency measures the corresponding transition frequency in another line [3,10]. For example, if a quantum-beat frequency of 160.4 cm^{-1} is measured on the S line at a detection frequency of 2080 cm^{-1} , the corresponding A transition frequency is $2080 - 160.4 = 1919.6 \text{ cm}^{-1}$. A single detection frequency does not have to correspond to a single frequency in another line [3]. The damping rate of the beat is related to the dephasing of the levels involved in the coherence and to the distribution of frequencies in other lines that map back to the detected transition frequency [3,46]. The amplitude of the QB is related to the coupling strength between the two transitions and the relative orientations between the transition dipole moments [50]. Quantum beats can, therefore, be used as a structural tool by comparing the relative orientations of different local oscillators within a molecule [20,48,51].

Accidental degeneracy beats can be used to extract different information from a system than quantum beats. Quantum beats can only be generated between states that can be prepared simultaneously and coherently [10]. Often, this is not possible. For example, suppose one wished to measure the anharmonicity of a vibrational transition with a quantum beat. In a third-order nonlinear experiment, laser pulse bandwidths that could couple both the 0–1 states and the 0–2 states directly would be required. For a typical vibration, this is $\sim 2000\text{--}4000 \text{ cm}^{-1}$. Even if excitation pulses with sufficient bandwidth were available, the 0–2 transition is only weakly allowed, and such an experiment would give almost no signal intensity. (A fifth-order experiment is required to measure the anharmonicity with a QB [36].) However, the anharmonicity of both the S and A transitions and the combination band shift, as well as the excited state line shapes can be determined in a spectrally resolved vibrational echo experiment. If the 0–1, 1–2, and combination band transitions are well resolved [Fig. 5(b)], the anharmonicities and spectral line shapes can be measured directly with a spectrally resolved vibrational echo experiment [52]. In the case where the spectral lines are not well resolved, the various anharmonic parameters can be determined from the beat frequencies [17]. The modulation depth of an ADB is a function of the amplitudes of the inhomogeneous lines of overlapping transitions at a particular frequency. By comparing the modulation depth of a particular ADB at a number of detection frequencies, it should be possible to reconstruct the shape and amplitude of the inhomogeneous lines of overlapping transitions.

Now consider the T_w scan calculated data in Fig. 8. The time slices in this figure are at the same frequencies as in Fig. 7. As shown previously, there are fewer beat frequencies in the T_w scan than in the τ scan. Two frequencies are easily resolvable in the regions where the 0–1 and combination bands overlap. These are the two pseudo-quantum-beat frequencies from Eqs. (2a) and (2c). In this particular system, these beat frequencies produce an ADB at $\sim 6 \text{ cm}^{-1}$. This is an ADB at the difference frequency between the two pseudo-quantum-beats in Eq. (2b). Because it is a low-frequency beat, it is not clearly resolvable in this presentation of the data. In places where the 0–1 and combination bands do not

overlap, there is only one frequency present. Like the QB seen in the τ -dependent scan, the pseudo-QB frequencies are not constant as a function of the detection frequency. The change in QB frequency as a function of the detection frequency is an indicator of the mechanism of inhomogeneous broadening.[3] The T_w -dependent scan is a good experiment to extract QB frequencies, because the number of different beat frequencies is reduced compared to a τ -dependent scan. Only in the spectral region where the 0–1 and combination band overlap are there multiple beat frequencies. T_w -dependent scans are a complementary technique to τ -dependent scans. For example, in a system where there is spectral overlap between the 0–1, 1–2, and combination bands, T_w -dependent scans can be used to accurately measure QB frequencies to determine correlations between transition frequencies, and the results can be combined with τ -dependent scans to extract anharmonicities.

As mentioned already, the beats in Eqs. (2a) and (2c) in the T_w scan are not necessarily pure quantum beats. While the population states in the T_w scan do not undergo phase evolution, each state does have an initial phase that is related to its previous coherence frequency on that particular quantum pathway. Because these pathways can have different initial coherence frequencies, the phases of each population state are not necessarily the same. The phase variations can influence the amplitude and phase of the observed beat. If one wishes to use the amplitude and phase of beats as a measure of the coupling strength and relative orientation of the coupled oscillators, then it is important to understand how these are influenced by spectral line overlap.

When computing the expected beat frequencies in Eqs. (2) in the T_w scan, the focus was on knowing how much a particular quantum pathway advanced in phase relative to another pathway. Because population states do not have an associated frequency, all population states were treated as zero-frequency states and the phase difference was computed between states that did evolve in frequency (ρ_{SA}^{II} and ρ_{SA}^{IV}) and states that did not evolve in frequency (ρ_{SS}^{I} , ρ_{00}^{I} , ρ_{00}^{II} , ρ_{SS}^{III} , and ρ_{AA}^{IV}). Because all population states were assigned a zero frequency, the frequency differences between ω_{SA}^{II} and all population states, and ω_{SA}^{IV} and all population states were the same. However, the initial phases of these population states were not considered.

The phase differences between each diagram can be calculated explicitly as they evolve in time. Since the echo signal is detected through a monochromator, the final coherence frequencies of all states are required to be equal to a particular detection frequency, and thus, only the phase behavior during the first two evolution periods needs to be considered. We denote the phases of each quantum pathway at the end of the second evolution period Φ_{Ia} , Φ_{Ib} , Φ_{IIa} , Φ_{IIb} , Φ_{II} , Φ_{IVa} and Φ_{IVb} , where the subscript refers to the type of diagram in Fig. 1:

$$\Phi_{\text{Ia}} = e^{-i\omega_{0S}^{\text{I}}\tau} e^{-i\omega_{SS}^{\text{I}}T_w}, \quad (12a)$$

$$\Phi_{\text{Ib}} = e^{-i\omega_{0S}^{\text{I}}\tau} e^{-i\omega_{00}^{\text{I}}T_w}, \quad (12b)$$

$$\Phi_{IIa} = e^{-i\omega_{0A}^{II}\tau} e^{-i\omega_{SA}^{II}T_w}, \quad (12c)$$

$$\Phi_{IIb} = e^{-i\omega_{0A}^{II}\tau} e^{-i\omega_{00}^{II}T_w}, \quad (12d)$$

$$\Phi_{III} = e^{-i\omega_{0S}^{III}\tau} e^{-i\omega_{SS}^{III}T_w}, \quad (12e)$$

$$\Phi_{IVa} = e^{-i\omega_{0A}^{IV}\tau} e^{-i\omega_{SA}^{IV}T_w}, \quad (12f)$$

$$\Phi_{IVb} = e^{-i\omega_{0A}^{IV}\tau} e^{-i\omega_{AA}^{IV}T_w}. \quad (12g)$$

Consider the terms that contribute to the pseudo-quantum-beat on the combination band. Interference between the terms in Eqs. (12f) and (12g) leads to a quantum beat, because these two quantum pathways end in the same final state. Interferences between Eq. (12f) and all the other population states lead to ADB's that have the same frequency as the QB in Eq. (2c), but are not QB's because these quantum pathways end in different final states than the quantum pathways in Eqs. (12f) and (12g). The observed beat is the difference between the coherence state Eq. (12f) and the sum of all the zero-frequency population states, Eqs. (12a), (12b), (12d), (12e), and (12g). Performing the vector summation yields the zero-frequency term

$$\begin{aligned} \sum_i A_i \Phi_i = & (A_{Ia} + A_{Ib}) e^{-i\omega_{0S}^I \tau} + A_{IIb} e^{-i\omega_{0A}^{II} \tau} + A_{III} e^{-i\omega_{0S}^{III} \tau} \\ & + A_{IVb} e^{-i\omega_{0A}^{IV} \tau}, \end{aligned} \quad (13)$$

where A_i is the amplitude of the beat component. In the case of ADB's, A_i is the amplitude of the inhomogeneous line at the initial coherence frequency of each transition. In the case of QB's A_i is a function of the coupling strength and the orientation of the oscillators. The overall expression for the combination band pseudo-QB is

$$\omega_1 = \Phi_{IVa} - \sum_i A_i \Phi_i. \quad (14)$$

There are two ways to see how this expression can give rise to different beat amplitudes and phases. The first way is to do the subtraction between Φ_{IVa} and each term in the sum. This produces five oscillatory terms with the same frequency but different initial phases and amplitudes. Addition of these oscillatory terms leads to either the constructive or the destructive interference and changes the overall initial phase of the beat. Changing the value of τ changes the initial phases of each oscillatory component, and, because each quantum pathway has a different initial coherence frequency, the manner in which all these terms interfere changes with τ , leading to overall changes in the amplitude and the phase. Alternatively, $\sum_i A_i \Phi_i$ can be thought of as the phase and amplitude of a local oscillator that Φ_{IVa} beats against as a function of T_w . Adjusting τ changes the phase and amplitude of the local oscillator, thereby changing the phase and depth of modulation of the observed beat.

Not all of the terms in Eq. (13) are present in all situations. With the exception of A_{IVa} , all of the A_i belong to

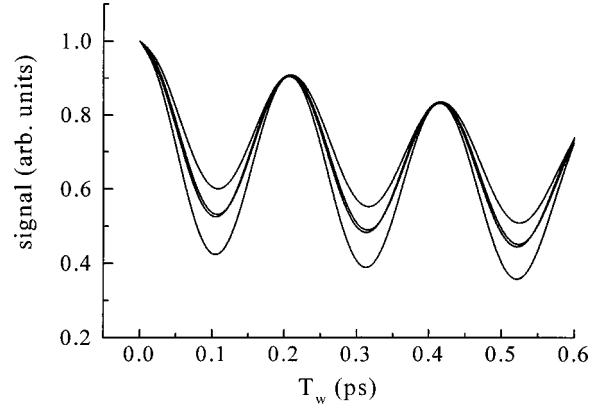


FIG. 9. Accidental degeneracy beat contribution to the modulation depth on the combination band. Accidental degeneracy beats with the same frequency as quantum beats but a different phase can influence the modulation depth seen in the signal in the case of wide inhomogeneous lines. The effect on the modulation depth is τ dependent. The bottom curve ($\tau=0.0$ ps) and the top curve ($\tau=1.663$ ps) are for wide inhomogeneous lines. When the combination band is well separated from the 0–1 and 1–2 line because the inhomogeneous lines are narrow (middle curves, $\tau=0.0$ and $\tau=1.663$ ps), the modulation depth of the beat is insensitive to τ .

ADB beat contributions, and accordingly, their amplitudes depend on the overlap of spectral lines. If there is no spectral line overlap, the value of these A_i is zero. In the case where the combination band is spectrally well resolved from all other peaks [Fig. 8(b)], Eq. (13) reduces to

$$\sum_i A_i \Phi_i = A_{IVa} e^{-i\omega_{0A}^{IV} \tau}. \quad (15)$$

For this case, the pseudo-quantum-beat in Eq. (2c) becomes a true quantum beat. The modulation depth in the spectrally resolved case is independent of the value of τ , because Φ_{IVa} and Φ_{IVb} have the same dependence on τ , and therefore always have the same initial phase.

Figure 9 presents a slice along the time axis for a T_w scan with the detection frequency set for the combination band for two values of τ and two levels of inhomogeneous broadening. In the case of extensive inhomogeneous broadening and overlapping spectral transitions on the combination band (bottom curve, $\tau=0.0$ ps; top curve, $\tau=1.663$ ps), the modulation depth of the beat depends strongly on the value of τ in the calculation. In contrast, the modulation depth is the same at two different values of τ in the case where the spectral lines are well separated (middle curves, $\tau=0.0$ and $\tau=1.663$ ps). These calculations illustrate that the modulation depth of a beat can be affected by spectral line overlap. Therefore, the modulation of the beat depth is not a quantum-beat effect. Rather, it is the result of an ADB with degenerate frequency but different initial phase. These calculations show that care must be taken when analyzing the modulation depth of beats to extract the coupling strength or relative orientation of local oscillators. A qualitatively similar analysis can be performed on the pseudo-quantum-beat of Eq. (2a). This is done in Appendix B.

So far, accidental degeneracy beats have only been discussed in the context of spectral overlap in nearby lines caused by inhomogeneous broadening. While this type of situation has been observed in a variety of experiments [3,17,26,30,53], ADB's are not restricted to such systems. Any system in which multiple dephasing frequencies can lead to a single rephasing frequency can exhibit ADB's. As an example, consider a homogeneously broadened uncoupled vibrational oscillator X that has a 0–1 transition frequency of 2000 cm^{-1} , a homogeneous linewidth of 5 cm^{-1} , and an anharmonicity of 45 cm^{-1} . An echo decay curve from such a system will show no oscillations, because the 0–1 and 1–2 lines are well separated and do not overlap. It is not possible for subensembles that have the same rephasing (and hence, emission) frequency to have different dephasing frequencies, because the 0–1 and 1–2 spectral lines do not overlap. If the same experiment is performed on a different molecule Y with a 0–1 transition frequency of 1955 cm^{-1} , homogeneous linewidth of 5 cm^{-1} , and anharmonicity of 45 cm^{-1} , again, no oscillations will be seen in the echo decay. However, if a solution containing both X and Y is used as the sample, the echo decay curve would show oscillations that correspond to a frequency of 45 cm^{-1} . In the mixture, it is possible for subensembles of molecules that have different dephasing frequencies to emit at the same frequency. At a detection frequency of 1955 cm^{-1} , the type-I quantum pathway of molecule Y dephases and rephases at 1955 cm^{-1} , while the type-III quantum pathway of molecule X dephases at 2000 and rephases at 1955 cm^{-1} . The fact that these are chemically different species makes no difference. The two different species act as the distinct “subensembles” that dephase at different frequencies but rephase at the same frequency.

ADB's of this kind have recently been observed in biomacromolecules [54]. Certain proteins, such as carbonmonoxymyoglobin (MbCO) are known to exist in a number of conformational substates [55,56]. These conformational substates are conformers of the same protein that have slightly different secondary and tertiary structure [57,58], and that interconvert with each other [55,59]. Because they have slightly different structure, these conformational substates can have different spectroscopic properties. While a single conformational substate may not have the required spectroscopic properties to exhibit ADB's, ADB's can be generated between different conformational states. ADB's have been observed between the A_1 and A_3 substates of MbCO [54]. The anharmonicity of the CO stretch in this system exceeds the inhomogeneous linewidths of the transitions, but in the region where the 1–2 line of the A_1 level overlaps with the 0–1 line of the A_3 line, beats at the frequency of the anharmonicity are observed.

V. CONCLUDING REMARKS

We have described in detail the nature of ADB's, which are a type of beat that can be seen in nonlinear spectroscopy. ADB's have many of the properties of quantum beats, but because ADB's result from an interference effect between different subensembles in the sample, their information content differs from that of quantum beats. A procedure has been

outlined that allows one to distinguish between accidental degeneracy beats and quantum beats. It has also been shown under what circumstances one expects to see ADB's. ADB's can manifest themselves as unique frequencies or as phase and amplitude contributions to quantum beat oscillations. ADB's are a direct consequence of spectral overlap in multilevel systems.

While this work has focused on the ADB's as they appear in vibrational echo experiments, ADB's can occur in any system where different quantum pathways with different phase evolution can lead to a single emission frequency. In experiments where the beat frequency is of primary interest, τ -dependent scans and T_w scans can be used in a complementary fashion to measure accurately all beat frequencies that are present in the system. Correlations between transition frequencies for coupled oscillators can most easily be measured in a spectrally resolved three-pulse stimulated photon echo experiment if the delay between the first two pulses is fixed and the delay between the second and third pulse is scanned (T_w scan). While ADB's can provide unique information about molecular systems, they can also complicate the nature of vibrational echo and other echo experiments. Therefore, it is important to consider their possible influence on observables when analyzing data from non-linear optical experiments.

ACKNOWLEDGMENTS

This work was supported by the National Institutes of Health (1R01-GM61137) and the National Science Foundation (DMR-0088942). One of the authors (K.A.M) was supported by Abbott Laboratories, Stanford.

APPENDIX A

In this appendix, expressions for the expected beat frequencies on the S manifold are derived from a system of inhomogeneously broadened anharmonic oscillators with correlated local mode frequencies. As discussed already in the text, it is necessary to have expressions for the energies of each level, and a model for the mechanism of spectral overlap. The eigenenergies used in the model system are listed in Eqs. (7) and (8), and the mechanism of spectral overlap is assumed to be inhomogeneous broadening caused by correlated variations in the local mode oscillator frequencies. First, consider τ -dependent beats. Only those density matrix elements with a final coherence frequency equal to the detection frequency ω_d are detected through the monochromator. The associated coherence frequencies for the density matrix elements ρ_{S0}^I , ρ_{S0}^{II} , $\rho_{2S,S}^{III}$, and $\rho_{A+S,A}^{IV}$ are ω_{S0}^I , ω_{S0}^{II} , $\omega_{2S,S}^{III}$, and $\omega_{A+S,A}^{IV}$, respectively. These are the rephasing frequencies of the diagrams, and as such $\omega_d = \omega_{S0}^I = \omega_{S0}^{II} = \omega_{2S,S}^{III} = \omega_{A+S,A}^{IV}$. Beats are produced at the differences between dephasing frequencies. The rephasing frequency of each diagram must be related to its corresponding dephasing frequency. Given the definition of a coherence frequency [33]

$$\omega_{ij} = \frac{E_i - E_j}{\hbar}, \quad (\text{A1})$$

where E_i and E_j are the energies of the states involved in the coherence and $2\pi\hbar$ is Planck's constant, and Eqs. (1), the dephasing frequencies for each diagram can be written as a function of the rephasing frequency

$$\omega_{0S}^I = \frac{E_0 - E_S}{\hbar} = -\frac{E_S - E_0}{\hbar} = -\omega_{0S}^I, \quad (\text{A2a})$$

$$\omega_{0A}^{II} = \frac{E_0 - E_A}{\hbar} = \frac{E_0 - (E_S - 2\delta\hbar)}{\hbar} = -\frac{(E_S - E_0) - 2\delta\hbar}{\hbar} = -(\omega_{S0}^{II} - 2\delta), \quad (\text{A2b})$$

$$\omega_{0S}^{III} = \frac{E_0 - E_S}{\hbar} = \frac{E_0 - (E_{2S} + \hbar\Delta_S - E_0 - E_S)}{\hbar} = -\frac{E_{2S} - E_S + \hbar\Delta_S}{\hbar} = -(\omega_{2S,S}^{III} + \Delta_S), \quad (\text{A2c})$$

$$\begin{aligned} \omega_{0A}^{IV} &= \frac{E_0 - E_A}{\hbar} = \frac{E_0 - (E_{A+S} + \hbar\Delta_C - E_S - E_0)}{\hbar} \\ &= -\frac{E_{A+S} + \hbar\Delta_C - (E_A + 2\hbar\delta)}{\hbar} \\ &= -\frac{(E_{A+S} - E_A) - 2\hbar\delta + \hbar\Delta_C}{\hbar} \\ &= -(\omega_{A+S,A}^{IV} - 2\delta + \Delta_C). \end{aligned} \quad (\text{A2d})$$

Substituting the above expressions for the first associated coherence frequencies into Eqs. (1) and remembering that $\omega_{S0}^I = \omega_{S0}^{II} = \omega_{2S,S}^{III} = \omega_{A+S,A}^{IV}$ yields

$$\omega_A = |(-\omega_{S0}^I) - [(\omega_{S0}^{II} - 2\delta)]| = 2\delta, \quad (\text{A3a})$$

$$\omega_B = |(-\omega_{S0}^I) - [-(\omega_{2S,S}^{III} + \Delta_S)]| = \Delta_S, \quad (\text{A3b})$$

$$\omega_C = |[(-\omega_{S0}^{II} - 2\delta)] - [(\omega_{2S,S}^{III} + \Delta_S)]| = 2\delta + \Delta_S, \quad (\text{A3c})$$

$$\omega_D = |(-\omega_{S0}^I) - [-(\omega_{A+S,A}^{IV} - 2\delta + \Delta_C)]| = 2\delta - \Delta_C, \quad (\text{A3d})$$

$$\omega_E = |[(-\omega_{S0}^{II} - 2\delta)] - [-(\omega_{A+S,A}^{IV} - 2\delta + \Delta_C)]| = \Delta_C, \quad (\text{A3e})$$

$$\begin{aligned} \omega_F &= |[(-\omega_{2S,S}^{III} + \Delta_S)] - [-(\omega_{A+S,A}^{IV} - 2\delta + \Delta_C)]| \\ &= 2\delta - \Delta_C + \Delta_S. \end{aligned} \quad (\text{A3f})$$

These are the expressions for the beat frequencies expected at a particular detection frequency. However, δ is a function of the detection frequency ω_d . Therefore, as ω_d is varied, δ varies, which changes the values of the beat frequencies in Eq. (A3).

For the beats in the T_w -dependent scan, the situation is more straightforward. The beat frequencies of the pseudo-QB's in Eqs. (2a) and (2c) are equal to the coherence frequencies of the second density matrix elements in the type-II

and type-IV quantum pathways. These frequencies can be computed from the definition in Eq. (A1). For the pseudo-QB in Eq. (2c), one should remember that the emission frequency is shifted by Δ_C from the 0–1 transition of the S line involved in the coherence of the second density matrix element in diagram type IVa. Once the beat frequencies in Eqs. (2a) and (2c) have been computed, taking the difference between the two gives the beat frequency for Eq. (2b).

APPENDIX B

In this appendix, the phase and amplitude behavior of the pseudo-QB on the 0–1 line in a T_w -dependent scan is described. The phase and amplitude changes in QB's have been observed experimentally in a variety of systems including nanocrystals [60] and solvated dyes [61]. However, possible ADB contributions to the behavior of these beats was not discussed. The overall description of the pseudo-QB on the 0–1 line is similar to that of the pseudo-QB on the combination band, but there are a few significant differences in the actual behavior between the pseudo-QB on the 0–1 line and the pseudo-QB on the combination band.

Equation (2a) can be rewritten to explicitly include each phase contribution to the zero frequency term

$$\omega_G = \Phi_{IIa} - \sum_i A_i \Phi_i \quad (\text{B1a})$$

with

$$\begin{aligned} \sum_i A_i \Phi_i &= (A_{Ia} + A_{Ib})e^{-i\omega_{0S}^I\tau} + A_{IIb}e^{-i\omega_{0A}^{II}\tau} + A_{III}e^{-i\omega_{0S}^{III}\tau} \\ &\quad + A_{IVb}e^{-i\omega_{0A}^{IV}\tau}. \end{aligned} \quad (\text{B1b})$$

As in the case of the pseudo-QB on the combination band, the difference between Φ_{IIa} and each term in the sum gives five beats with the same frequency but different initial phases. Changing the value of τ in the experiment changes the initial phases of each term, giving a different overall phase and amplitude to ω_G as each term interferes with the others. The behavior of both ω_G and ω_I as τ is changed is the same in the case where there is large spectral overlap between the 0–1, 1–2, and combination bands. However, the behavior of the two beats is different when the various spectroscopic lines are well resolved. Unlike the combination band pseudo-QB ω_I where $\sum_i A_i \Phi_i = A_{IVa}e^{-i\omega_{0A}^{IV}\tau}$ in the well-resolved spectroscopic line case, when the 0–1 line is well separated from other lines, Eq. (B1b) reduces to

$$\sum_i A_i \Phi_i = (A_{Ia} + A_{Ib})e^{-i\omega_{0S}^I\tau} + A_{IIb}e^{-i\omega_{0A}^{II}\tau}. \quad (\text{B2})$$

All three of these terms come from diagrams that end with the same final state as in diagram IIa. As such, they can influence the phase and amplitude of the QB on the 0–1 line, even when there is no spectral overlap. Despite the fact that Eq. (B1a) is a true QB when there is no spectral overlap

between the 0–1 and other lines, the value of τ can still affect the amplitude of the beat. Substituting Eq. (B2) into Eq. (B1a) gives

$$\begin{aligned}\omega_G &= \Phi_{IIa} - (A_{Ia} + A_{Ib})e^{-i\omega_{0S}^I\tau} - A_{IIb}e^{-i\omega_{0A}^{II}\tau} \\ &= A_{IIa}e^{-i\omega_{0A}^{II}\tau}e^{-i\omega_{SA}^{II}T_w} - (A_{Ia} + A_{Ib})e^{-i\omega_{0S}^I\tau} - A_{IIb}e^{-i\omega_{0A}^{II}\tau} \\ &= e^{-i\omega_{0A}^{II}\tau}(A_{IIa}e^{-i\omega_{SA}^{II}T_w} - (A_{Ia} + A_{Ib})e^{-i(\omega_{0S}^I - \omega_{0A}^{II})\tau} - A_{IIb}).\end{aligned}\tag{B3}$$

As can be seen in Eq. (B3), the frequency of the beat in a T_w -dependent scan is the frequency difference between the S

and A states, and the maximum depth of the beat changes as a function of τ and at the frequency difference between the S and A states. Whether the combination band beat is a pseudo-QB or a true QB can be tested by seeing if the modulation depth of the beat is independent of τ . In the case of the beat on the 0–1 line, whether the pseudo-QB is a true QB can be tested by comparing the frequency of the beat with the frequency of the change in maximum modulation depth as a function of τ . If the two frequencies are not the same, then the beat on the 0–1 line has ADB contributions. Equation (B3) shows that one must be careful when using the QB amplitude to extract coupling information, because the beat depth is sensitive to the value of τ used in the experiment.

-
- [1] K. D. Rector, A. S. Kwok, C. Ferrante, R. S. Francis, and M. D. Fayer, *Chem. Phys. Lett.* **276**, 217 (1997).
- [2] M. Gruebele and A. H. Zewail, *J. Chem. Phys.* **98**, 883 (1993).
- [3] D. E. Thompson, K. A. Merchant, and M. D. Fayer, *J. Chem. Phys.* **115**, 317 (2001).
- [4] W. P. de Boeij, M. S. Pshenichnikov, and D. A. Wiersma, *Chem. Phys.* **233**, 287 (1998).
- [5] G. M. Clore and A. M. Gronenborn, *Prog. Nucl. Magn. Reson. Spectrosc.* **23**, 43 (1991).
- [6] S. Tsuda, *J. Crystallogr. Soc. Jpn.* **38**, 84 (1996).
- [7] D. M. Besemann, N. J. Condon, K. M. Murdoch, W. Zhao, K. A. Meyer, and J. C. Wright, *Chem. Phys.* **266**, 177 (2001).
- [8] M. Berg, C. A. Walsh, L. R. Narasimhan, K. A. Littau, and M. D. Fayer, *J. Chem. Phys.* **88**, 1564 (1988).
- [9] M. Berg and D. A. Vander Bout, *Acc. Chem. Res.* **30**, 65 (1997).
- [10] R. T. Carter and J. R. Huber, *Chem. Soc. Rev.* **29**, 305 (2000).
- [11] A. Tortschanoff, K. Brunner, C. Warmuth, and H. F. Kauffmann, *J. Chem. Phys.* **110**, 4493 (1999).
- [12] T. Joo, Y. Jia, J. Y. Yu, M. J. Lang, and G. R. Fleming, *J. Chem. Phys.* **104**, 6089 (1996).
- [13] I. D. Abella, N. A. Kurnit, and S. R. Hartmann, *Phys. Rev.* **141**, 391 (1966).
- [14] A. I. Lvovsky and S. R. Hartmann, *Laser Phys.* **6**, 535 (1996).
- [15] O. Golonzka, M. Khalil, N. Demirdoven, and A. Tokmakoff, *Phys. Rev. Lett.* **86**, 2154 (2001).
- [16] T. S. Yang, P. Vohringer, D. C. Arnett, and N. F. Scherer, *J. Chem. Phys.* **103**, 8346 (1995).
- [17] K. D. Rector, A. S. Kwok, C. Ferrante, A. Tokmakoff, C. W. Rella, and M. D. Fayer, *J. Chem. Phys.* **106**, 10027 (1997).
- [18] E. F. McCormack and E. Sarajlic, *Phys. Rev. A* **63**, 023406 (2001).
- [19] Y. Tang, J. P. Schmidt, and S. A. Reid, *J. Chem. Phys.* **110**, 5734 (1999).
- [20] P. Hamm, M. Lim, W. F. Degrado, and R. M. Hochstrasser, *J. Chem. Phys.* **112**, 1907 (2000).
- [21] G. Bartels and A. Stahl, *Phys. Status Solidi B* **206**, 325 (1998).
- [22] H. Fidder, F. Tschirschwitz, O. Duhr, and E. T. J. Nibbering, *J. Chem. Phys.* **114**, 6781 (2001).
- [23] T. Kohmoto, Y. Fukuda, and M. Kunitomo, *Phys. Lett. A* **277**, 233 (2000).
- [24] P. Waltner, A. Materny, and W. Kiefer, *J. Appl. Phys.* **88**, 5268 (2000).
- [25] A. Tokmakoff, A. S. Kwok, R. S. Urdahl, R. S. Francis, and M. D. Fayer, *Chem. Phys. Lett.* **234**, 289 (1995).
- [26] K. A. Merchant, D. E. Thompson, and M. D. Fayer, *Phys. Rev. Lett.* **86**, 3899 (2001).
- [27] M. C. Asplund, M. T. Zanni, and R. M. Hochstrasser, *Proc. Natl. Acad. Sci. U.S.A.* **97**, 8219 (2000).
- [28] M. Koch, J. Feldmann, G. von Plessen, E. O. Gobel, P. Thomas, and K. Kohler, *Phys. Rev. Lett.* **69**, 3631 (1992).
- [29] D. Zimdars, A. Tokmakoff, S. Chen, S. R. Greenfield, M. D. Fayer, T. I. Smith, and H. A. Schwetman, *Phys. Rev. Lett.* **70**, 2718 (1993).
- [30] P. Hamm, M. Lim, and R. M. Hochstrasser, *Phys. Rev. Lett.* **81**, 5326 (1998).
- [31] R. Vreeker, M. W. L. Bovy, and M. Glasbeek, *Phys. Rev. B* **29**, 4869 (1984).
- [32] H. Torii and M. Tasumi, *J. Chem. Phys.* **97**, 86 (1992).
- [33] S. Mukamel, *Principles of Nonlinear Optical Spectroscopy* (Oxford University Press, New York, 1995).
- [34] L. R. Narasimhan, Y. S. Bai, M. A. Dugan, and M. D. Fayer, *Chem. Phys. Lett.* **176**, 335 (1991).
- [35] D. Weber, W. Petri, U. Woggon, C. F. Klingshim, S. Shevel, and E. O. Gobel, *Phys. Rev. B* **55**, 12 848 (1997).
- [36] P. Hamm, M. Lim, M. Asplund, and R. M. Hochstrasser, *Chem. Phys. Lett.* **301**, 167 (1999).
- [37] M. D. Fayer, *Elements of Quantum Mechanics* (Oxford University Press, New York, 2001).
- [38] J. T. Fourkas, H. Kawashima, and K. A. Nelson, *J. Chem. Phys.* **103**, 4393 (1995).
- [39] M. Khalil and A. Tokmakoff, *Chem. Phys.* **266**, 213 (2001).
- [40] C. A. Walsh, M. Berg, L. R. Narasimhan, and M. D. Fayer, *J. Chem. Phys.* **86**, 77 (1987).
- [41] M. T. Zanni, M. C. Asplund, and R. M. Hochstrasser, *J. Chem. Phys.* **114**, 4579 (2001).
- [42] S. M. Gallagher, A. W. Albrecht, T. D. Hybl, B. L. Landin, B. Rajaram, and D. M. Jonas, *J. Opt. Soc. Am. B* **15**, 2338 (1998).
- [43] J. D. Hybl, A. A. Ferro, and D. M. Jonas, *J. Chem. Phys.* **115**, 6606 (2001).
- [44] N. Demirdoven, M. Khalil, O. Golonzka, and A. Tokmakoff, *J. Phys. Chem. A* **105**, 8030 (2001).
- [45] K. K. Lehmann, *J. Chem. Phys.* **96**, 8117 (1992).

- [46] S. T. Cundiff, *Phys. Rev. A* **49**, 3114 (1994).
- [47] W. H. Press, S. A. Teukolsky, W. T. Vetterling, and B. P. Flannery, *Numerical Recipes in C: The Art of Scientific Computing*, 2nd ed. (Cambridge University Press, New York, 1992).
- [48] O. Golonzka, M. Khalil, N. Demirdoven, and A. Tokmakoff, *J. Chem. Phys.* **115**, 10814 (2001).
- [49] W. M. Zhang, V. Chernyak, and S. Mukamel, *J. Chem. Phys.* **110**, 5011 (1999).
- [50] O. Golonzka and A. Tokmakoff, *J. Chem. Phys.* **115**, 297 (2001).
- [51] C. Scheurer, A. Piryatinski, and S. Mukamel, *J. Am. Chem. Soc.* **123**, 3114 (2001).
- [52] M. C. Asplund, M. Lim, and R. M. Hochstrasser, *Chem. Phys. Lett.* **323**, 269 (2000).
- [53] K. D. Rector and M. D. Fayer, *Int. Rev. Phys. Chem.* **17**, 261 (1998).
- [54] K. A. Merchant, D. E. Thompson, Q.-H. Xu, and M. D. Fayer (unpublished).
- [55] W. S. Caughey, H. Shimada, M. C. Choc, and M. P. Tucker, *Proc. Natl. Acad. Sci. U.S.A.* **78**, 2903 (1981).
- [56] H. Shimada and W. S. Caughey, *J. Biol. Chem.* **257**, 11893 (1982).
- [57] J. G. N. Phillips, M. L. Teodoro, T. Li, B. Smith, and J. S. Olson, *J. Phys. Chem. B* **103**, 8817 (1999).
- [58] J. Vojtechovsky, K. Chu, J. Berendzen, R. M. Sweet, and I. Schlichting, *Biophys. J.* **77**, 2153 (1999).
- [59] J. B. Johnson, D. C. Lamb, H. Frauenfelder, J. D. Muller, B. McMahon, G. U. Nienhaus, and R. D. Young, *Biophys. J.* **71**, 1563 (1996).
- [60] R. W. Schoenlein, D. M. Mittleman, J. J. Shiang, A. P. Alivisatos, and C. V. Shank, *Phys. Rev. Lett.* **70**, 1014 (1993).
- [61] W. P. de Boeij, M. S. Pshenichnikov, and D. A. Wiersma, *J. Chem. Phys.* **105**, 2953 (1996).